Cytokinesis and postabscission midbody remnants are regulated during mammalian brain development

Katrina C. McNeely[a,b] and Noelle D. Dwyer[a,1]

[a]Department of Cell Biology, University of Virginia School of Medicine, Charlottesville, VA 22908; and [b]Neuroscience Graduate Program, University of Virginia School of Medicine, Charlottesville, VA 22908

Edited by Carol Ann Mason, Columbia University, New York, NY, and approved March 5, 2020 (received for review November 13, 2019)

Building a brain of the proper size and structure requires neural stem cells (NSCs) to divide with tight temporal and spatial control to produce different daughter cell types in proper numbers and sequence. Mammalian NSCs in the embryonic cortex must maintain their polarized epithelial structure as they undergo both early proliferative divisions and later neurogenic divisions. To do this, they undergo a polarized form of cytokinesis at the apical membrane that is not well understood. Here, we investigate whether polarized furrowing and abscission in mouse NSCs are regulated differently at earlier and later stages and in a cytokinesis mutant, *Kif20b*. This mutant was previously shown to have microcephaly and elevated apoptosis of NSCs. We developed methods to live image furrow ingression and midbody abscission in NSCs within cortical explants. We find that polarized furrow ingression occurs at a steady rate and completes in ∼15 min at two different ages. However, ingression is slower in a subset of *Kif20b* mutant NSCs. Abscission is usually observed on both sides of the midbody and takes 65 to 75 min to complete. Surprisingly, abscission is accelerated in the *Kif20b* mutant NSCs. Postabscission midbody remnants are observed at the apical membranes of daughter cells and are much more abundant in early-stage cortices. After NSC divisions in vitro, midbody remnants are more often retained on the daughter cells of early proliferative divisions. Altogether, these results suggest that regulation of abscission timing and midbody remnants in embryonic NSCs may influence proper brain growth and structure.

cytokinesis | midbody | microcephaly | mouse | stem cell

To build a brain of the proper size and structure, neural stem cells (NSCs) must proliferate rapidly to produce billions of daughter cells in a short developmental time window and generate different daughter cell types at specific times. NSCs are tall, thin cells that are highly polarized, extending radially to contact the pia on the basal side. Their apical membranes ("apical endfeet") are joined by junctions and form the walls of the lateral ventricles. Their nuclei move within them during the cell cycle in a process called interkinetic nuclear migration. Nuclei move to the basal side for S phase and to the apical membrane for M phase and must carefully regulate the positioning of mitosis and cytokinesis (Fig. 1*B*). This nuclear movement creates a pseudostratified epithelium as NSCs proliferate. During early development, NSCs perform symmetric proliferative divisions to produce two NSC daughters and expand the stem cell pool. Later, NSCs increase neurogenic divisions, producing neuron daughters that differentiate, migrate basally, and never divide again (1, 2). Errors in these divisions can result in brains that are too small or have abnormal structure (2, 3). How the NSCs accomplish these divisions and control the balance of proliferative and neurogenic daughter fates is a subject of intense study.

As they divide, the NSCs must faithfully segregate genomes and organelles to their daughters and confer proper daughter fates while maintaining their polarity and the integrity of the epithelium. To do this, NSCs undergo a polarized form of cytokinesis that is poorly understood: first, the furrow ingresses from basal to apical, and second, abscission occurs at the apical membrane. Cleavage is near perpendicular to the apical membrane (4). While many studies have shown that disrupting the perpendicular cleavage plane can deplete the stem cell pool or disrupt cortical structure (5–8), the regulation of furrow ingression itself has not been thoroughly addressed.

The basic mechanisms of cytokinetic abscission have been established primarily from studies in single-cell models (9, 10). After chromosome segregation, the central spindle promotes cleavage furrow ingression and compacts its microtubules into a structure called the midbody within the intercellular bridge. The center of the midbody microtubule bundle contains overlapping plus ends embedded in a dense matrix, which appears as a bulge on live imaging. The midbody contains over 450 proteins that assemble within the central bulge or on the lateral flanks of microtubule bundles that extend on each side of the central bulge (10–13). This structure serves as a platform to mediate abscission, the process of severing the intercellular bridge. Abscission involves both microtubule disassembly and plasma membrane constriction by endosomal sorting complexes required for transport (ESCRT)-III filaments, leading to scission of the midbody flanks (14, 15). After abscission, the central bulge remains intact and is called the midbody remnant (MBR). Potentially, MBRs could transmit signals to neighboring cells by surface binding or internalization as "MBsomes" (16–18). Evidence from developing worms and flies as well as mammalian stem cell lines suggests that temporal and spatial regulation of abscission can influence daughter cell polarity and fate (19–26). It is unclear whether these simpler systems accurately model abscission dynamics in the developing

Significance

During prenatal brain development, neural stem cells must divide to produce billions of daughter cells. At early stages, they produce more stem cells. Later, they produce neurons. Errors in their divisions can result in abnormal brains. We address whether cytokinesis—cleavage furrowing and intercellular bridge severing (abscission)—occurs differently at different ages and in a small-brained mouse mutant of a kinesin motor protein gene. We developed a method to image neural stem cells undergoing cytokinesis in brain explants. We found that remnants of severed intercellular bridges are more likely to remain on daughter cells at earlier ages. In the kinesin gene mutant, bridge severing occurs faster. These findings suggest that precise regulations of cytokinesis are important during early brain development.

Author contributions: K.C.M. and N.D.D. designed research; K.C.M. performed research; K.C.M. and N.D.D. analyzed data; and K.C.M. and N.D.D. wrote the paper.

The authors declare no competing interest.

This article is a PNAS Direct Submission.

[1]To whom correspondence may be addressed. Email: ndwyer@virginia.edu.

This article contains supporting information online at https://www.pnas.org/lookup/suppl/doi:10.1073/pnas.1919658117/-/DCSupplemental.

First published April 9, 2020.

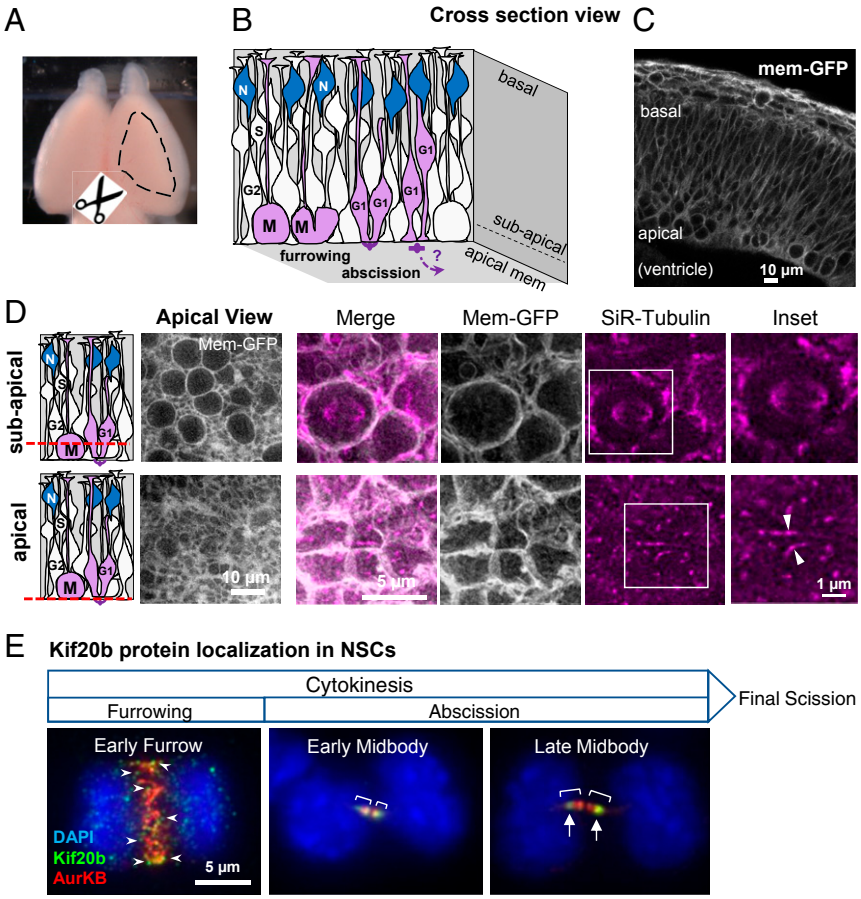

Fig. 1. Imaging cytokinesis in NSCs of developing cortex. (*A*) Embryonic mouse brain with dashed outline showing area of cortex dissected for cortical slab preparation. (*B*) Schematic of NSCs forming the pseudostratified epithelium of the developing cerebral cortex. NSCs undergo interkinetic nuclear migration. Their nuclei move basally for S phase and apically for mitosis (M). Mitosis, furrowing, and abscission occur at the apical membrane. Abscission completes during G1 phase. N, postmitotic neurons. (*C*) Cross-section image of E12.5 mouse cortex expressing membrane-GFP shows the dense packing of NSCs in the epithelium. Round cells in mitosis can be seen close to the apical surface. (*D*) Schematics and images of cortical slabs labeled with membrane-GFP (green fluorescent protein) and SiR-Tubulin, viewing the apical membrane en face, at two different imaging planes (red dashed lines). *Upper* shows the subapical plane where the rounded mitotic cells with larger cell diameters and mitotic spindles are located. *Lower* shows the apical plane where apical endfeet and cell junctions are located and where the midbody forms and abscission occurs. Arrowheads point to the central bulges of two different midbodies. (Scale bars in *D* also apply to panels directly above.) (*E*) Endogenous Kif20b immunostaining in dissociated fixed embryonic cortical mouse NSCs shows changes in Kif20b localization (green) at progressive stages of cytokinesis. A cell in the early furrowing stage shows many Kif20b puncta (arrowheads) on the central spindle, which is labeled by AuroraB kinase (red). Chromatin is labeled by DAPI (4′,6-diamidino-2-phenylindole) (blue). A cell at early midbody stage of abscission shows Kif20b localized on the entire AuroraB-positive midbody flanks (brackets), but at late midbody stage, Kif20b becomes enriched on the outer flanks (arrows) near the constriction sites. Furrowing starts during anaphase, and abscission progresses during telophase and completes with final scission in G1. Kif20b staining is undetectable in *Kif20b* mutant NSCs (27). (Scale bar in *E* applies to all three images.) Image credit: Michael Fleming (University of Virginia School of Medicine, Charlottesville, VA).

brain, where polarized stem cells must alter the balance of proliferation and differentiation during development.

Previously, we showed that a loss-of-function mutation of the Kinesin-6 *Kif20b* in mice causes microcephaly, partly due to elevated apoptosis of NSCs (27–29). Kif20b protein shows a dynamic localization during cytokinesis that suggests that it could play roles in furrow ingression or abscission. During the first part of cytokinesis, furrowing, Kif20b protein localizes to the central spindle (in anaphase). In the second part of cytokinesis, abscission, Kif20b is found first on the midbody flanks (in telophase) and later at the constriction sites where final scission will occur (in late telophase or G1) (Fig. 1*E*) (27, 30–32). We showed that, in HeLa cells, Kif20b depletion caused subtle disruptions of furrowing speed, midbody maturation, and abscission timing but did not prevent abscission completion (30). This raised the question of whether Kif20b loss causes more severe defects of cytokinesis in NSCs than in HeLa cells. In fixed brains of *Kif20b* mutants, we found no changes in the proportions or positions of mitotic or S-phase NSCs (27). Cleavage furrow angles were not different from controls, and binucleate cells were not detected. However, the cortical NSCs did have a reduced midbody index and wider, disorganized midbodies. Together, these data suggested that loss of Kif20b specifically causes defects in cytokinesis and that regulation of cytokinesis in NSCs is critical for proper brain development.

Here, we address two main questions: whether cytokinesis is differentially regulated in NSCs during early proliferative and later neurogenic stages of cortical development, and whether loss of Kif20b disrupts the kinetics of NSC furrowing or abscission. Since the durations of furrowing and abscission in cortical NSCs had not been measured before, we developed methods to quantitatively analyze these events in NSCs through live imaging in intact cortical explants and compared different developmental stages. Using both live and fixed preparations, we find that abscission in NSCs usually occurs on each midbody flank sequentially and that MBRs persist at the apical membrane.

This is consistent with the idea that the MBR has the potential to induce or carry signals to daughter cells or neighbor cells post-abscission. Interestingly, MBRs are observed more often with proliferative divisions than neurogenic divisions. Furthermore, Kif20b seems to regulate both furrow ingression speed and abscission timing in cortical NSCs. Together, these data add to a growing body of work showing that subtle alterations of abscission timing and MBR regulation can influence daughter fates and tissue development.

Results

Furrowing and Abscission Kinetics of Embryonic NSCs Can Be Analyzed in Intact Cortical Explants. To better understand cytokinesis events and kinetics of NSCs in their polarized epithelial structure and to identify specific defects in cytokinesis mutants, we developed a method to live image both cytokinetic furrowing and abscission in intact cortical explants. Both furrowing and abscission occur near the apical membrane. Therefore, instead of cutting cross-section slices, we dissect a flat "slab" of neocortex from membrane-GFP transgenic mice (Fig. 1*A*) and culture it in a glass-bottom dish to view the apical membrane en face. The cultured cortical slabs, which are ∼150- to 200-μm thick, are incubated with SiR-Tubulin (Silicon–Rhodamine–Tubulin), a cell-permeable dye that fluoresces in far red when it binds polymerized microtubules. Thus, we can image fields containing many NSC apical endfeet. Cells in mitosis are rounded up with a bipolar spindle, making them easily detectable using membrane-GFP or SiR-Tubulin (Fig. 1 *B–D*, subapical planes). Midbodies form at the apical membrane (Fig. 1 *B–D*, apical planes). Live time-lapse imaging of NSC cytokinesis can be done by collecting *z* stacks of images at time points 3 min apart for single-color imaging and 15 min apart for two-color imaging. These time intervals and short exposure times are both essential for maintaining the health of the NSCs. We live imaged cytokinesis in both control and *Kif20b* mutant cortical explants at two ages.

Kif20b May Facilitate Furrow Ingression in Cortical NSCs. NSC cleavage furrowing controls the plane of division and positions the midbody at the apical membrane. Here, we set out to determine the kinetics of furrowing and if they change with developmental stage or loss of Kif20b. Mitotic cells are easy to identify near the apical membrane owing to their large, spherical shape. Cytokinesis begins with the cell elongating parallel to the apical membrane before the furrow initiates on the basal side and ingresses asymmetrically toward the apical membrane. In control cells, furrow ingression proceeds smoothly at a constant rate (Fig. 2 *A*, *a*). Under these conditions, the rate of furrow ingression for control NSCs is 0.4 μm/min (Fig. 2 *B* and *E*, black lines) and takes ∼15 min to complete (Fig. 2 *D* and *G*, control) at both E11.5 (proliferative divisions) and E13.5 (neurogenic divisions). The elongation is also unchanged during development (Fig. 2 *C* and *F*, black lines). Most *Kif20b*$^{-/-}$ NSCs behave like controls, and none show furrow regression (Fig. 2 *A*, *b*). However, a subset of cells furrows abnormally, taking 24 min to complete (Fig. 2 *A*, *c*, *B*, red line, and *E*, red line). This subset of slow cells causes the median time to furrow completion to be increased by 3 min in *Kif20b* mutant brains (Fig. 2 *D* and *G*). These data show that 1) furrowing kinetics do not significantly change between E11.5 and E13.5 and that 2) Kif20b is not required for cleavage furrowing but may help to ensure continuous rapid furrow ingression.

Abscission Is Accelerated in *Kif20b* Mutants. It was unknown how long abscission takes following mitosis in cortical NSCs. Therefore, we analyzed the spatial and temporal dynamics of abscission in NSCs in the cortical explant system. Fig. 3*A* shows a representative NSC at an early stage of abscission, with a wide pre-abscission midbody. A rotated image stack (*x–z* view) illustrates how the midbody microtubule bundle bridges the two daughter cells across their cell junction. At later stages of abscission (Fig. 3*B*), the midbody is narrower, and sometimes, microtubule bundle thinning can be seen on one flank (Fig. 3*B*, open arrowheads). By live time-lapse, with two-color imaging of the membrane and microtubules, we were able to follow NSCs through abscission. Abscission involves both the disassembly of microtubules and scission of membrane on the midbody flanks. We cannot detect the midbody membrane since the membrane-GFP label (myristoylated-GFP) does not enrich in the midbody. Therefore, we defined abscission completion as the time point when microtubules were disassembled on a midbody flank, ascertained when the SiR-Tubulin signal intensity decreased to background level (Fig. 3*C*). Microtubule thinning prior to complete disassembly was sometimes detected (Fig. 3*C*, 60′).

The timing of abscission has been linked to daughter cell fates in fly germline stem cells and mouse embryonic stem cells (24, 26). To ask if abscission duration changes as brain development proceeds, we measured the time from midbody formation to the first abscission at two different ages. At E11.5, when divisions are predominantly proliferative, we found that abscission duration ranged widely from 15 to 120 min, with a mean of 57 min (Fig. 3*D*). At E13.5, when neurogenic divisions have increased, the range of durations was 15 to 105 min, and the mean was 47 min (Fig. 3*E*). A cumulative frequency plot shows a trend to faster abscission at E13.5 (Fig. 3*F*, solid lines). These data suggest that abscission duration may decrease as development proceeds. However, we were not able to test this at a later age when divisions are primarily neurogenic since the thicker cortical slab explants from older brains (>400-μm thick at E15.5) do not remain healthy in these cultures.

Based on our previous findings in fixed brains, that *Kif20b* mutant NSCs have abnormal midbody structure and increased apoptosis (27, 28), we hypothesized that some *Kif20b* mutant NSCs have delayed or failed abscissions. To our surprise, in live imaging, every mutant NSC observed was able to complete abscission. Moreover, the average time from midbody formation to the first abscission was not delayed but accelerated compared with controls by 18 min at E11.5 and 9 min at E13.5 (Fig. 3 *D* and *E*). Comparing the cumulative frequency plots of *Kif20b* mutant abscissions at the two ages shows that they almost overlie (Fig. 3*F*, dashed lines), suggesting a loss of developmental regulation. Thus, Kif20b regulates the duration of abscission, particularly at E11.5 when symmetric proliferative divisions predominate.

Reports vary on whether abscission occurs on one midbody flank or both flanks. Studies in dissociated cells, such as HeLa and MDCK (Madin–Darby canine kidney), showed that ESCRT-III recruitment occurs on both flanks followed by sequential, bilateral abscission (15, 33). By contrast, unilateral abscission and midbody inheritance by one daughter cell were reported in the worm embryo (23), fly germline (22), and fly imaginal disk epithelium (34). Furthermore, abscission duration and frequency of midbody release varied in different mammalian neural cell lines (20). These conflicting reports suggest that bilateral abscission may depend on cell type or developmental context. Therefore, we wanted to use our system of live imaging with SiR-Tubulin to determine the frequency of cortical NSCs abscission on one or both midbody flanks, the relative timing, and if this varies with developmental stage or when Kif20b is absent. Interestingly, MBRs have been found in cerebrospinal fluid of early (E10.5) mouse embryos (35), and it was suggested that bilateral abscission is important for symmetric fates in early proliferative NSC divisions. Surprisingly, we detected bilateral abscission just as often in E13.5 divisions as E11.5 divisions, in at least 60% of the cases (Fig. 4 *A* and *B*). The two abscissions usually were captured in sequential images, but occasionally, both took place within one time-lapse interval. The median time between the first and second event was 30 min at E11.5 and 15 min at E13.5, with a maximum

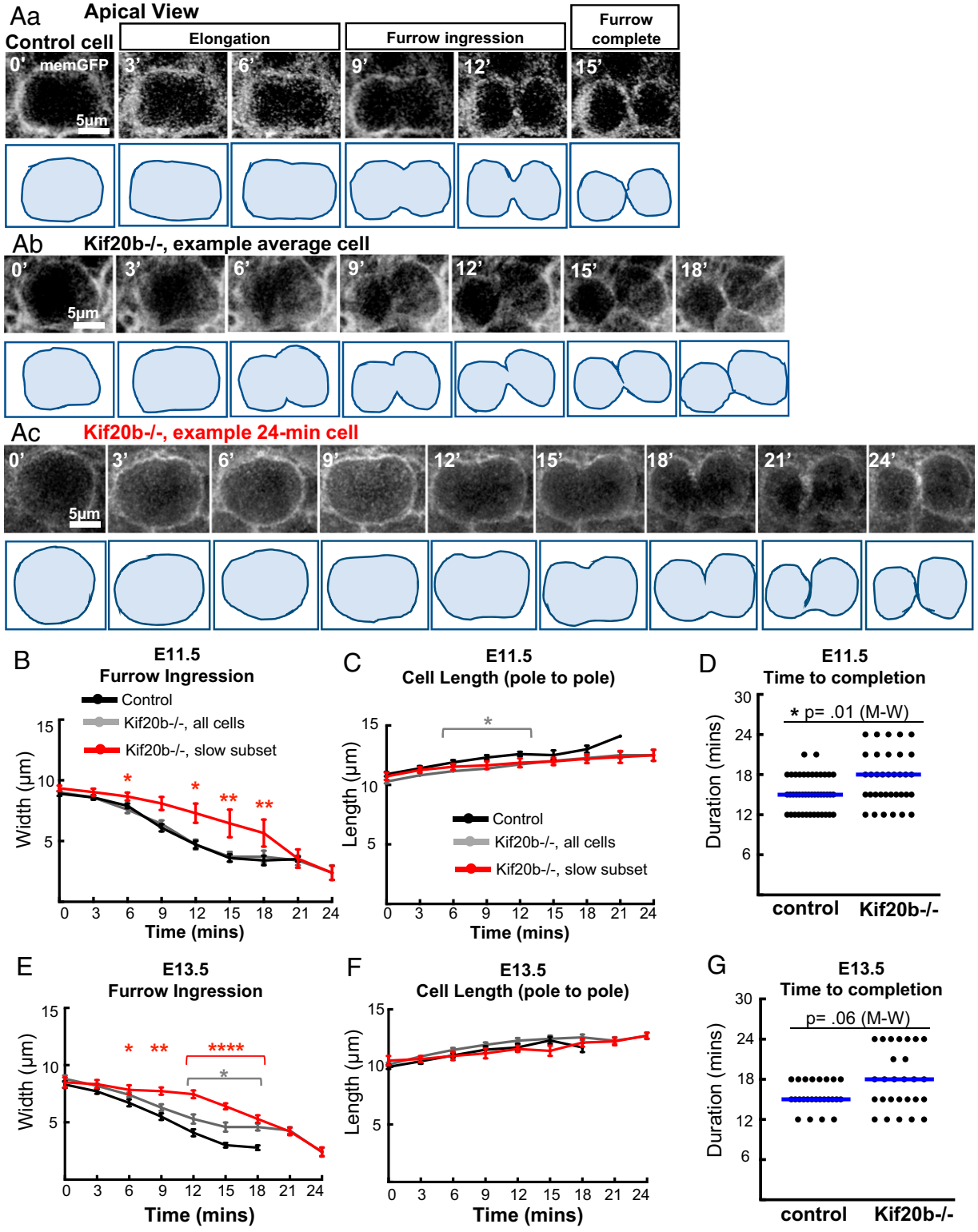

Fig. 2. In *Kif20b* mutant brains, a subset of NSCs furrows more slowly. (*A*) Representative images and traced silhouettes of cytokinetic furrow ingression in one E13.5 control (*A*, *a*), one normally furrowing *Kif20b* mutant (–/–) NSC (*A*, *b*), and one abnormally slow furrowing mutant NSC (*A*, *c*). Furrowing was considered complete when no additional narrowing of furrow width occurred and the membrane between sister cells appeared continuous. Times shown in minutes (′). (*B*, *C*, *E*, and *F*) Furrow width and pole to pole length were plotted over time in E11.5 (*B* and *C*) and E13.5 (*E* and *F*) control (black lines) and *Kif20b*$^{-/-}$ (gray lines) cortical slab explants. Most *Kif20b*$^{-/-}$ cells furrow at a similar rate to controls, but a subset (red lines) furrows more slowly and takes 24 min to complete. (*D* and *G*) Time to furrow completion was increased in E11.5 and E13.5 *Kif20b* mutant cortices, with a subset of NSCs taking 24 min to complete. Blue lines are medians. (*B*–*G*) E11.5: $n = 43$ control cells from two brains (one +/– and one +/+), $n = 35$ total *Kif20b*$^{-/-}$ cells from two brains, $n = 5$ *Kif20b*$^{-/-}$ cells in slow subset (red lines); E13.5: $n = 25$ control cells (from two +/– brains and one +/+ brain), $n = 27$ total *Kif20b*$^{-/-}$ cells from three brains, $n = 7$ *Kif20b*$^{-/-}$ cells in slow subset (red lines). For (*D* and *G*) *P* values from Mann–Whitney (M-W) test. *$P < 0.05$ (Student's *t* test); **$P < 0.01$ (Student's *t* test); ****$P < 0.0001$ (Student's *t* test).

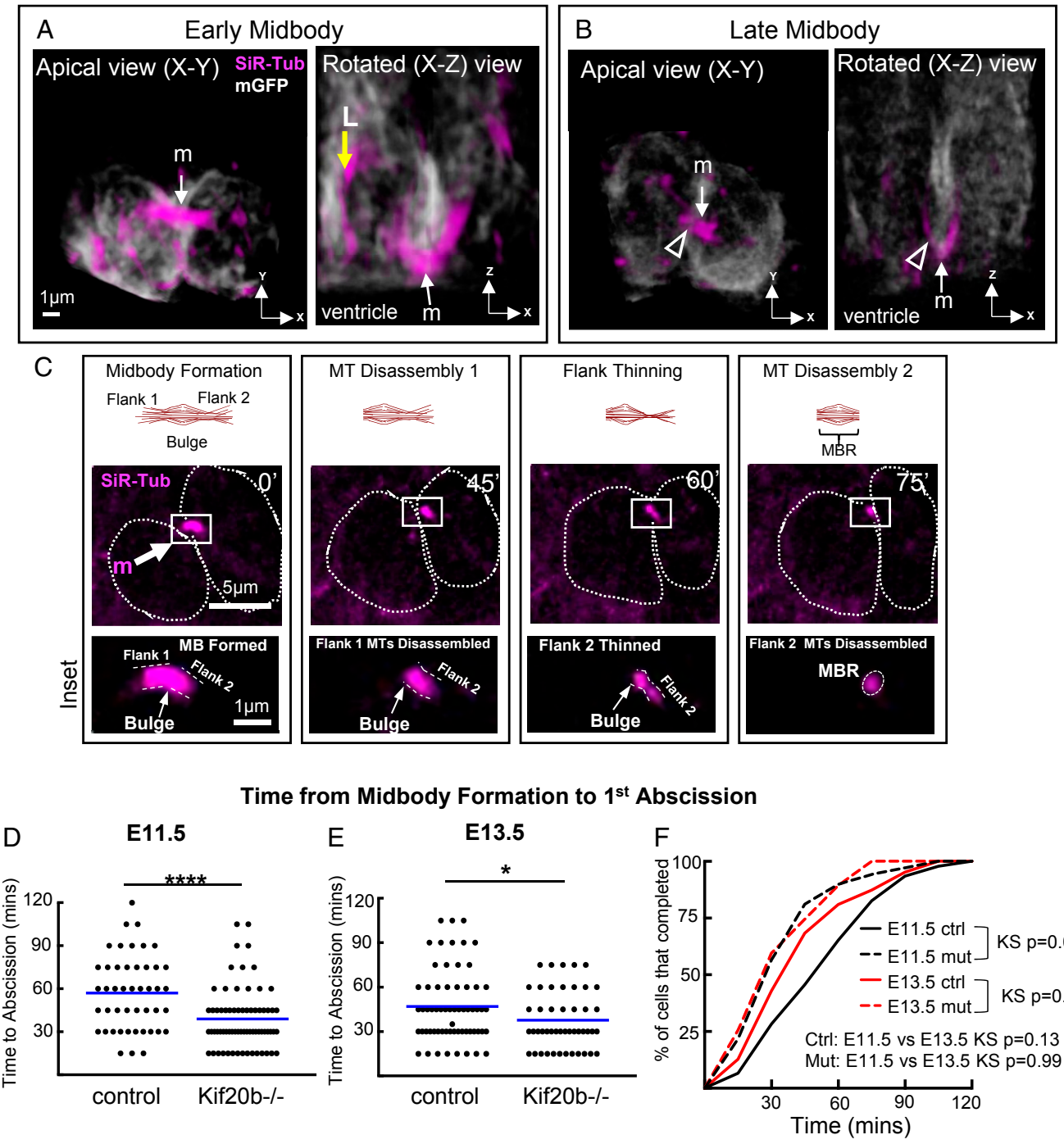

Fig. 3. Abscission is accelerated in *Kif20b* mutant cortex. (*A* and *B*) The 3D renderings of NSCs at early (*A*) or late (*B*) midbody stage labeled by membrane-GFP and SiR-Tubulin viewed from both the apical view (imaging plane) and the rotated lateral view. Midbodies (m; arrows) form at the apical membrane (ventricular surface). Late midbody has thinning on one flank (open arrowheads). L, longitudinal microtubule bundles. MT, microtubules. Time shown in minutes ('). (Scale bar in *A* applies to all images in *A* and *B*.) (*C*) Schematic and images of time-lapse imaging of an NSC midbody undergoing abscission with central bulge and flanks indicated in *Insets*. Distinct steps seen here are midbody formation (m), microtubule disassembly on flank 1 (first abscission), flank 2 thinning, and microtubule disassembly on flank 2 (second abscission). Dotted circular outlines show the shapes of sister cell plasma membranes at a subapical plane where cells are the widest. Scale bars in *C* apply to all images in that row. (*D* and *E*) Time from midbody formation to first abscission is reduced in *Kif20b*$^{-/-}$ NSCs at both ages (E11.5 and E13.5). Blue lines show means. (*F*) Cumulative frequency plots show that E11.5 *Kif20b*$^{-/-}$ NSCs abscission timing curve is shifted to the left and has an altered shape. For E11.5, $n = 46$ +/+ cells (from four brains), $n = 69$ *Kif20b*$^{-/-}$ cells (four brains). For E13.5, $n = 63$ +/+ cells (five brains), $n = 47$ –/– cells (three brains). KS, Kolmogorov–Smirnov. *$P < 0.05$ (Student's *t* test); ****$P < 0.0001$ (Student's *t* test).

of 90 min (Fig. 4 *C* and *D*). Kif20b loss does not seem to alter the frequency of bilateral abscission (Fig. 4 *A* and *B*), but it does significantly reduce the time between first and second abscissions in E11.5 NSCs (Fig. 4*C*). In total, the mean time to complete bilateral abscissions was 23 min less in the *Kif20b* mutants at E11.5 and 13 min less at E13.5 (Fig. 4 *E*–*G*). Together, these data suggest that bilateral abscission is common in NSCs of the early cortex and that Kif20b does not regulate its frequency but

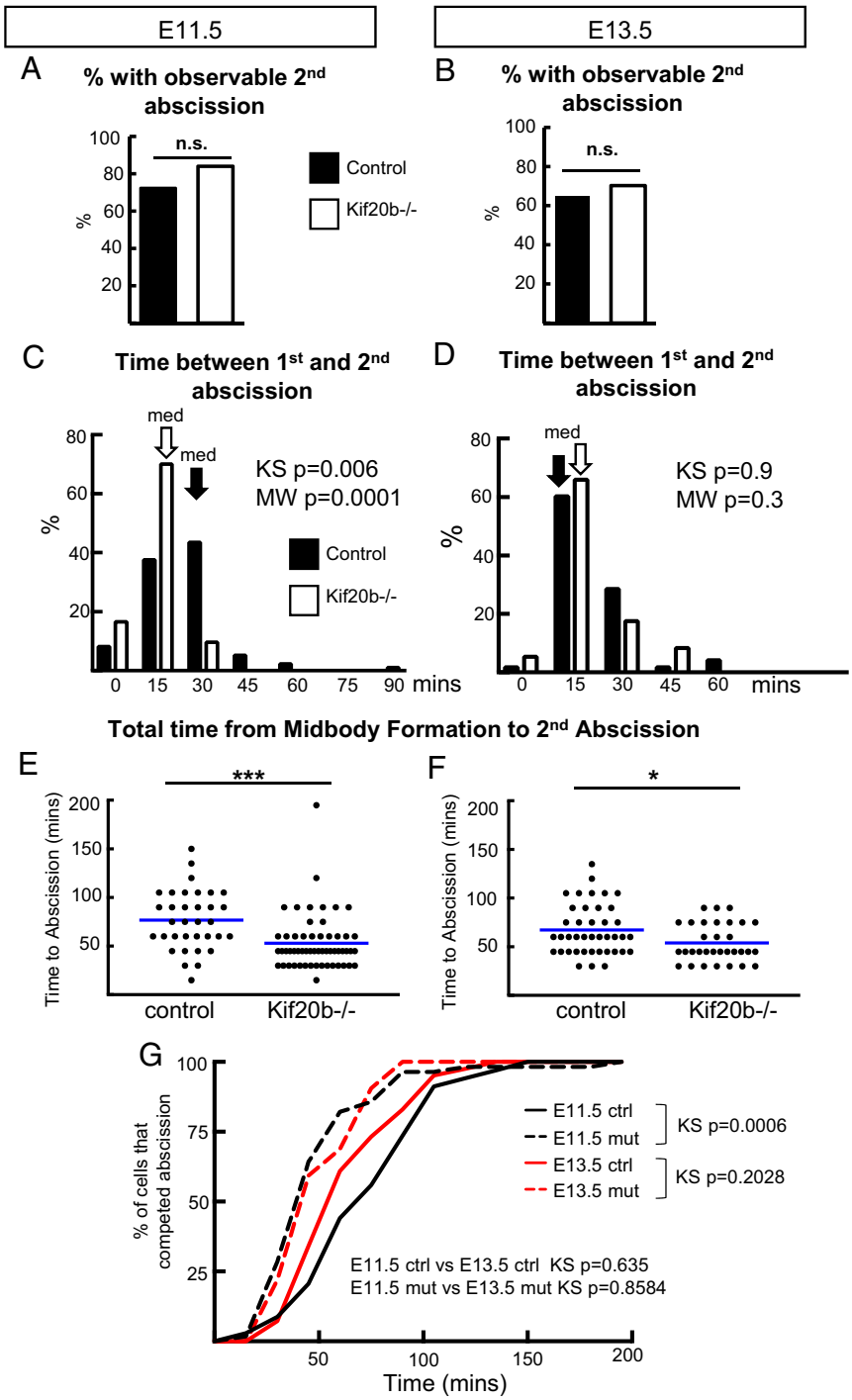

Fig. 4. Sequential abscissions on both flanks are observed in most NSC divisions and occur faster in *Kif20b*$^{-/-}$ brains. (*A* and *B*) Using the same methods as in Fig. 3, scoring abscission by the disassembly of SiR-Tubulin on midbody flanks, the second abscission on the other flank was observable in more than 60% of NSCs in E11.5 and E13.5 cortices, regardless of genotype. (*C* and *D*) At E11.5, the second abscission was usually detected within 30 min of the first abscission in control NSCs but within 15 min in *Kif20b*$^{-/-}$ NSCs. At E13.5, the second abscission was within 15 min in both control and mutant cells. Black and white arrows indicate medians (med) for control and mutant, respectively. (*E* and *F*) The total time from midbody formation to completion of bilateral abscissions is reduced in *Kif20b* mutant NSCs at both ages. Blue lines show means. (*G*) Cumulative frequency curves of total time to second abscissions of E11.5 and E13.5 *Kif20b*$^{-/-}$ NSCs (dashed lines) are shifted to the left of control curves (solid lines). For E11.5, $n = 34$ +/+ (four brains), $n = 56$ *Kif20b*$^{-/-}$ cells (four brains). For E13.5, $n = 41$ +/+ (five brains), $n = 32$ –/– cells (three brains). KS, Kolmogorov–Smirnov; MW, Mann–Whitney; n.s., not significant (Fisher's exact test). *$P < 0.05$ (Student's *t* test); ***$P < 0.001$ (Student's *t* test).

regulates the timing of its completion. These findings in the early mammalian neuroepithelium appear different from the unilateral abscission seen in fly larval epithelium (34) but similar to observations of sequential bilateral abscission in HeLa and dissociated MDCK cells (15, 33).

MBRs Are Abundant in Early Cortex and Associated with Proliferative NSC Divisions. Postabscission MBRs have been shown to adhere to plasma membranes of daughter or neighbor cells and may influence cell polarity or proliferation (16, 17, 36). We wanted to ask whether MBRs of cortical NSCs remain on the apical membrane

after abscission and whether this changes across development. We could not follow postabscission MBRs in live time-lapse imaging due to the strong microtubule labeling throughout the tissue, and therefore, we used the same cortical slab explant preparation as described in Fig. 1*A* but fixed the cortical slabs for immunostaining. MBRs can be identified in fixed cortical slabs or dissociated NSCs by immunostaining for protein markers of the midbody central bulge and flanks. Preabscission midbodies have the central bulge (marked by Citron Kinase or Cep55) and two flanks (marked by Aurora Kinase B or Survivin). Postabscission MBRs retain the

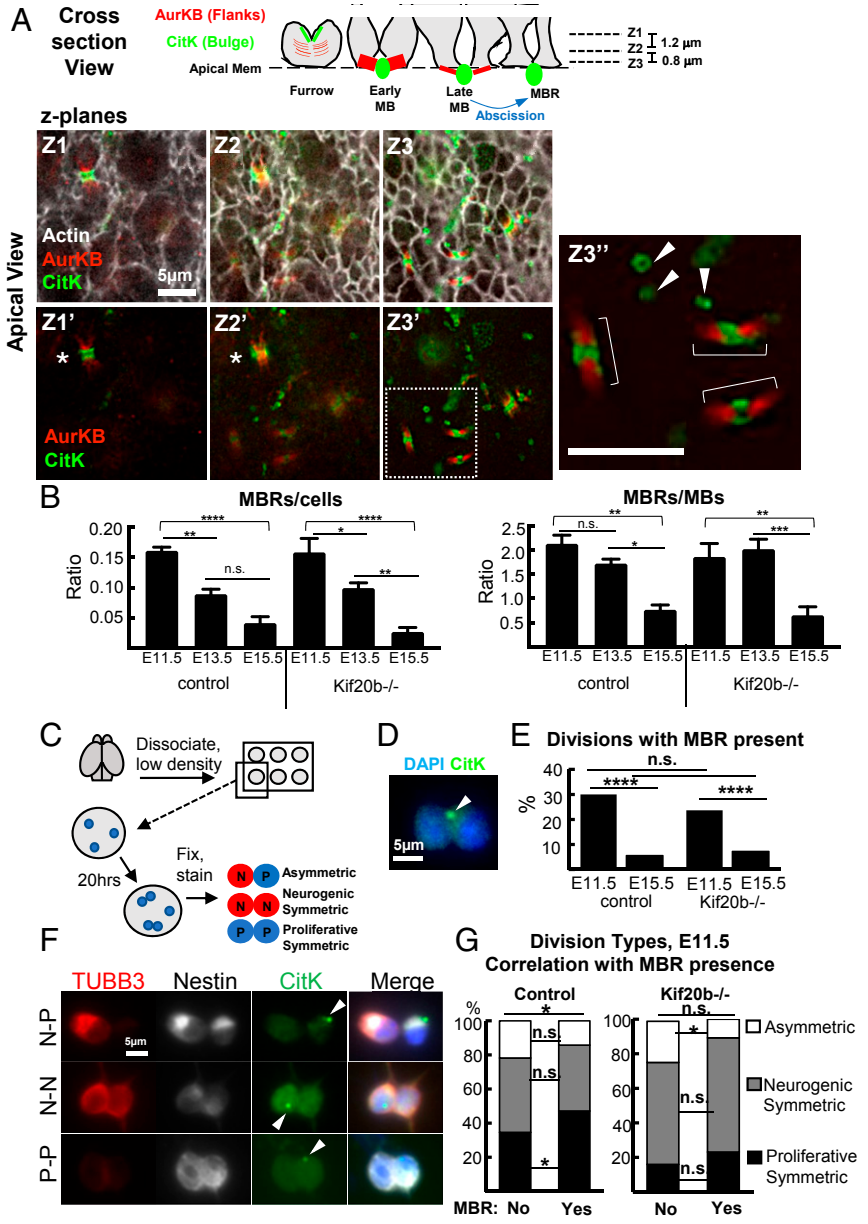

Fig. 5. MBRs are detected at the apical membrane and correlated with early proliferative symmetric divisions. (*A*) Schematic and three image *z* planes (Z1 to Z3) of a field of apical membrane of a fixed E11.5 cortical slab show many NSC junctions (actin; white), a late furrow in planes Z1 to Z2 (asterisks), preabscission midbodies (MB) (brackets; Z3″), and postabscission MBRs in planes Z2 to Z3 (arrowheads; Z3″). AurKB labels preabscission midbody flanks. CitK labels both preabscission midbody central bulge and postabscission MBRs. (Scale bar in Z3″, 5 µm. Scale bar in Z1 applies to Z1–Z3′.) (*B*) Many more MBRs are seen on E11.5 and E13.5 apical membranes than E15.5 normalized to either cell number or midbody number. For E11.5, $n = 4$ control (three +/– and one +/+), $n = 4$ *Kif20b*$^{-/-}$ brains. For E13.5, $n = 5$ control (three +/– and two +/+), $n = 5$ –/– brains. For E15.5, $n = 3$ control (one +/– and two +/+), $n = 4$ –/– brains. *$P < 0.05$ (ANOVA); **$P < 0.01$ (ANOVA); ***$P < 0.001$ (ANOVA); ****$P < 0.0001$ (ANOVA). (*C*) Schematic of pair cell assay. (*D*) Pair of daughters of an E11.5 NSC division in vitro, with an associated MBR labeled by CitK (arrowhead), chromatin labeled by DAPI (4′,6-diamidino-2-phenylindole). (*E*) E11.5 NSC division pairs are more likely to have an MBR present than E15.5 division pairs in both control and *Kif20b*$^{-/-}$ NSCs. (*F*) Images of three division pairs of different fate types, each with an MBR detected (CitK+; arrowheads). Note that newborn neurons still have Nestin protein inherited from the mother NSC during the first day after division (56). N, neuron (Nestin+, Tubb3+); P, progenitor (Nestin+, Tubb3–). (Scale bar applies to all panels in *F*.) (*G*) The proportions of division types were compared in pairs with or without an MBR present. Control NSC division pairs with MBRs are more often proliferative symmetric (P-P). *Kif20b*$^{-/-}$ NSCs have reduced proliferative symmetric divisions with or without an MBR present. For E11.5, $n = 394$ control (three +/– and two +/+ brains), $n = 272$ *Kif20b*$^{-/-}$ divisions (four brains). For E15.5, $n = 241$ control (four +/– brains and one +/+ brain), $n = 280$ *Kif20b*$^{-/-}$ divisions (five brains). n.s., not significant. For individual category distributions in *E* and *G*, *$P < 0.05$ (Fisher's exact test); ****$P < 0.0001$ (Fisher's exact test). For overall distributions in *G*, *$P < 0.05$ (χ^2 test).

central bulge but have lost the flanks due to scission (*SI Appendix*, Fig. S1). On the apical membranes of NSCs in cortical slabs, both preabscission midbodies (Fig. 5*A*, brackets) and postabscission MBRs (Fig. 5*A*, arrowheads) are observed (Fig. 5*A*). We quantified MBRs on the apical surface at three ages, when divisions progress from primarily proliferative (E11.5) to mixed (E13.5) to primarily neurogenic (E15.5). Strikingly, approximately fourfold more MBRs are observed on E11.5 and E13.5 cortices than E15.5 (Fig. 5*B*). Kif20b loss does not alter the frequency of observed MBRs or the developmental difference. These data suggest that E15.5 brains alter their regulation of either MBR release or degradation but that Kif20b is not required for this change.

To more precisely quantify MBR association with individual NSC divisions, we modified the established NSC "pair cell" assay (37). NSCs were plated as single cells at clonal density and fixed the next day to assess whether MBRs are present on newly divided daughter pairs (Fig. 5 *C* and *D*). First, we found that, with control NSCs, ∼30% of E11.5 division pairs have an MBR, while only 5% of E15.5 division pairs do, an approximately sixfold difference (Fig. 5*E*). *Kif20b*$^{-/-}$ divisions pairs showed a similar developmental difference. Second, to ask whether MBRs were associated with particular daughter fate outcomes, we scored MBR presence in the different types of divisions of E11.5 NSCs. By colabeling with NSC marker Nestin and neuron marker tubulin-beta-III (Tubb3), the division pairs were classified as proliferative symmetric (two NSC daughters), neurogenic symmetric (two neuron daughters), or asymmetric (Fig. 5*F*). Interestingly, E11.5 division pairs that have an associated MBR are more likely to be proliferative symmetric (Fig. 5*G*, control). In the *Kif20b* mutant, this association is no longer statistically significant; however, this may be precluded by a significant reduction in the percentage of divisions that are proliferative symmetric compared with control NSCs (Fig. 5*G*, *Kif20*$^{-/-}$ bars). The reason for this is unknown but does not seem to be due to a loss of MBRs. Together with the in vivo quantifications of MBRs, these data show that MBRs are more prevalent in the early cortex and are more associated with early proliferative NSC divisions than later neurogenic divisions. Furthermore, Kif20b loss does not disrupt MBR production or prevalence in the early cortex.

Discussion

The polarized form of cytokinesis in embryonic cortical NSCs is poorly understood but may influence the segregation of organelles and apical fate determinants to daughter cells as they make fate choices. Recent findings that mutations in *Kif20b* and other midbody genes cause microcephaly in humans and mice suggest that brain development is especially sensitive to defects in cytokinesis (27, 38–42). To elucidate these issues, we developed methods to quantitatively analyze furrowing and abscission in NSCs of the developing cerebral cortex. Here, we addressed 1) whether cytokinesis parameters differ as development proceeds from more proliferative to more neurogenic divisions and 2) how the loss of kinesin Kif20b affects cytokinesis kinetics in the developing cortex. While furrow ingression kinetics do not change significantly with developmental stage, abscission processes in cortical NSCs do seem to be developmentally regulated. MBRs are more prevalent on the apical membranes of early-stage cortices and are more associated with proliferative NSC divisions than neurogenic divisions. Kif20b loss did not disrupt this developmental regulation of MBRs. However, the loss of Kif20b resulted in accelerated abscission. In addition, *Kif20b* mutant NSCs make fewer symmetric proliferative divisions. In the context of emerging data in both the neurogenesis and cytokinesis fields, these data suggest that subtle changes in the kinetics of cytokinesis or in the handling of MBRs could influence NSC daughter fates.

Through live time-lapse experiments, we found that Kif20b loss causes subtle dysregulation of abscission timing in both HeLa cells (30) and NSCs (this paper). In our previous analyses of fixed cell populations, we more frequently observed early-stage midbodies than late-stage mature midbodies in both *Kif20b* mutant NSCs and Kif20b-depleted HeLa cells (27, 28, 30). Together, these findings are consistent with the hypothesis that the late steps of abscission proceed more quickly in the absence of Kif20b. Exactly how Kif20b regulates abscission timing is not clear, but prior work suggests two main hypotheses. First, previous work by us and others shows that Kif20b can cross-link microtubules in vitro (31) and help bundle axonal microtubules in neurons (43). Thus, when Kif20b is absent, the reduced cross-linking of midbody microtubules could allow easier removal or disassembly at the abscission sites. Second, we previously identified a role for Kif20b in keeping NSC midbodies aligned with the apical membrane (27, 28). Hypothetically, if Kif20b links midbody microtubules to apical junction proteins, it could mediate tension on the midbody, which has been shown to affect abscission timing in HeLa cells (44). Additional hypotheses, currently without evidence, are that Kif20b might localize an unidentified cargo that regulates timing of ESCRT-III filament formation or that Kif20b could be part of the abscission checkpoint (45, 46). Interestingly, the related Kinesin-6 family member Kif20a/MKLP2 was reported to act in the abscission checkpoint, although involving a tail sequence not shared by Kif20b (47). Much more work is needed to understand how Kif20b and other mechanisms control midbody maturation and abscission timing in different cell types and developing tissues.

It is possible that altered abscission timing in NSCs could affect daughter fates or proliferation. Our data showed a trend for faster abscission at E13.5 than E11.5. Consistent with this, in an embryonic stem cell line, faster abscission was correlated with more differentiation and reduced potency (26). Interestingly, delayed abscission timing in the fly germline is important for maintaining stem cell fate (24). In HeLa cells, failed abscission causes persistent intercellular bridges, midbody regression/binucleation, or cell death (48), but faster abscission has no morphological or fate consequences (49). Furthermore, *Kif20b* mutant NSCs at E11 display the same accelerated abscission as control E13 NSCs and also have a significant reduction in proliferative symmetric divisions, about half the control percentage. This is accompanied by a concomitant increase in neurogenic divisions. It is tempting to speculate that the faster abscission in the *Kif20b* mutant contributes to the early loss in proliferative symmetric divisions, depleting the stem cell pool and resulting in microcephaly. However, we cannot rule out some other role of *Kif20b* in promoting symmetric proliferative divisions.

In addition to the loss of symmetric proliferative divisions, the *Kif20b* mutant brains have increased apoptosis that is mediated by p53 (28). When the p53 knockout was crossed into the *Kif20b* mutant, the NSC apoptosis was prevented, and the microcephaly was partly but not fully rescued. Hence, the remaining microcephaly may be due to the loss of early symmetric proliferative divisions demonstrated here. Future work will determine if this fate change is also p53-dependent.

We found that the number of MBRs at the apical membrane is much higher in early-stage cortices, even when normalized for number of divisions. The mechanism for this developmental difference is not known. However, the correlation of MBR presence with proliferative symmetric fates is intriguing because MBRs have been proposed to contain fate determinants and to have signaling roles, either from the cell surface or from being engulfed as MBsomes by daughter or neighbor cells (16, 17, 35). An attractive hypothesis is that an early symmetric proliferative division of a cortical NSC would occur through bilateral abscission on both flanks and release of the MBR extracellularly, whereas a later asymmetric neurogenic division could result from unilateral abscission on one flank and midbody inheritance by the other daughter, promoting asymmetric fates. However, our data argue against this possibility by showing that bilateral abscission is observed with similar frequency at two different developmental time

points. Another possible explanation for the difference in MBR persistence at early and late ages is that the disposal of MBRs is regulated differently by E15.5 NSCs. It is not known if NSCs have similar mechanisms for MBR engulfment and degradation as other cell types (16, 50), but differential regulation of these processes in early- vs. late-stage stem cells could alter the ability of MBRs to influence the polarity or fates of progeny. While Kif20b does not seem to regulate the persistence of MBRs, this assay may be used in future cytokinesis mutant analyses to discover the roles and regulation of MBRs. The composition and signaling capacity of MBRs in stem cells and other dividing cell types require further investigation.

In conclusion, subtle changes in early NSC abscission regulation could affect daughter cell fate choices that would have long-term consequences for global neurogenesis. In cortical NSCs, fate-signaling events at the apical membrane happen concurrently with abscission and could be affected by abscission duration or midbody/MBR positioning. These include new apical junction building, notch signaling across it, centrosome docking, and ciliogenesis. As these events occur, the release of the MBR could serve to either remove fate determinants from daughter cells or to transmit them to neighbor cells. Future studies in multiple stem cell types and developing tissue systems are needed to further elucidate how developmental regulation of cytokinesis contributes to stemness, differentiation, and building tissues and organs.

Materials and Methods

Mice. The animal protocol was approved by the University of Virginia Institutional Animal Care and Use Committee, and the colonies were maintained in accordance with NIH guidelines. The morning of the vaginal plug was considered embryonic day (E)0.5. All embryos were harvested by cesarean section, and littermate controls were used when possible. The *Kif20b*^{magoo} (*Kif20b*$^{-/-}$) mutant mouse was generated in an ENU screen (*N*-ethyl-*N*-nitrosourea) (29). It carries a loss-of-function splice site mutation that reduces the protein to undetectable levels (27). The *Kif20b* mutant mouse was crossed with both the mT/mG reporter line (Jax stock #007576) and Sox2-Cre mice (JAX stock #008454) (51, 52) to produce mice that expressed plasma membrane-localized GFP.

Cortical Slab Explant Culture for Cleavage Furrow and Abscission Live Imaging. E11.5 or E13.5 embryos were removed from the uterus and dissected in cold 1× PBS (phosphate-buffered saline). After decapitation, the skull was removed, and #5 forceps were used to pinch out the cortices. Each hemisphere was placed into a glass-bottom dish (MatTek P35G-1.0–20-C) containing 50 nM SiR-Tubulin (Cytoskeleton CY-SC002) in Final Culture Medium (described below). The hemispheres were then trimmed to create flat cortical slabs and flipped over so that the apical surface faced the glass. Each dish was placed in a humidifying chamber and into a 37 °C incubator with 5% CO_2 overnight (approximately 15 h). The next day, the cortices were removed from the incubator, and the 50 nM SiR-Tubulin–containing medium was removed. Matrigel (Corning 356237; 1:3 dilution in Final Culture Medium) was added on top of the cortical slab. High-vacuum grease (Fisher 14–635-5D) was placed on the edge of the glass-bottom dish in four spots, and a coverslip (Fisher 12–545-100) was placed over the top of the cortical slab explant. Gentle pressure was applied to the coverslip at the spots where the vacuum grease was placed. The dish was put back into the incubator, and the Matrigel was allowed to solidify for 5 min. Final culture medium with 2% 4-(2-hydroxyl)-1-piperazineethanesulfonic acid (Gibco 15630080) was added to the dish, and then, imaging was performed. An Applied Precision (GE) DeltaVision with Truelight Deconvolution and softWorx suite 5.5 image acquisition software equipped with a heating plate and 40× objective (numerical aperture 1.53) was used for time-lapse image acquisition; *z* stacks of images ∼10-μm deep (*z* steps 0.4 μm) were taken every 15 min for abscission and every 3 min for cleavage furrowing for up to 6 h. To minimize phototoxicity, the neutral density filter was set at 32% or lower, and the exposure time was kept to a minimum (<0.1 ms per slice). The total cortical slab thickness varied by age (E11.5: ∼150 μm, E13.5: ∼200 μm). To confirm that 50 nM SiR-Tubulin treatment did not cause mitotic arrest, we fixed and stained for phosphohistone H3, a mitotic marker: we found no difference in the mitotic index after SiR-Tubulin treatment. Additionally, in time-lapse movies, the cells that failed to complete furrowing or abscission were similar between genotypes and were excluded from analyses.

Cleavage Furrow Ingression and Abscission Analysis. Deconvolved full *z* stacks and maximum intensity projection images were analyzed using ImageJ. For cleavage furrowing, membrane-GFP cells were identified in mitosis by their characteristic round shape. Time 0 was considered the last time point before furrowing began. The length and width of the cell were measured until furrow completion; it was considered complete when 1) there was no additional subsequent narrowing of the furrow tips and 2) the membrane between sister cells appeared continuous. For abscission, time 0 was midbody formation as ascertained by SiR-Tubulin appearance (compact microtubule bundles). Abscission completion was scored as the time point when there was complete removal of microtubules on a midbody flank ascertained when the SiR-Tubulin signal intensity decreased to background level. Midbody membrane scission was shown to be temporally coincident with midbody flank microtubule disassembly by several previous publications using differential interference contrast or phase imaging of cell lines in two-dimensional dissociated cultures (33, 44, 53); however here, we cannot rule out the possibility that the midbody plasma membrane might remain connected for some period of time after the microtubules are gone. Still image stacks for three-dimensional (3D) renderings (Fig. 3 *A* and *B*) were acquired using longer exposure times and finer *z* steps (0.2 μm) on E13.5 cortical slabs incubated in higher concentration of SiR-Tubulin (200 nM); 3D renderings were created in PerkinElmer Volocity 3D Image Analysis Software (access to Volocity was provided by Barry Hinton, University of Virginia School of Medicine, Charlottesville, VA).

Immunohistochemistry on Fixed Cortical Slabs. This method was previously described (54). Briefly, the skulls were opened to reveal the cortices, and the head was fixed for 20 min in 2% paraformaldehyde (PFA) for E11.5 and 4% PFA for E15.5. Cortical hemispheres were pinched off, placed in slide wells (catalog nos. 70366–12, 70366–13), and trimmed to flat pieces of neocortex (slabs) as outlined by the dashed line in Fig. 1*A*. Total cortical slab thickness varied by age (E11.5: ∼150 μm, E15.5: ∼400 μm). The cortical slabs were briefly fixed again with PFA before immunostaining. After coverslipping, images were acquired using the 60× objective on the Applied Precision (GE) DeltaVision microscope.

Pair Cell Assay for NSC Divisions. The pair cell assay for dissociated cortical NSC divisions was adapted from refs. 37 and 55. E11.5 or E15.5 mouse embryos were removed from the uterus and placed in Hibernation Medium (Gibco Hibernate-E A12476-01), and cortices were dissected out. Meninges were removed from E15.5 cortices. The cortices were then placed into a 15-mL conical tube for dissociation. Papain from Worthington kit (Worthington Biochemical Corporation LK003150) was added, and cortices were placed on a rotator at 37 °C for 30 min (E11.5) or 45 min (E15.5). The cortices were then manually dissociated with a 1-mL Rainin pipette followed by centrifugation at 4 °C at 1,300 rpm for 10 min. The cell pellet was then washed with Dulbecco's Modified Eagle Medium (DMEM) (Invitrogen 11960–051). The wash and centrifugation steps were repeated three times. After the final wash, the cells were resuspended in Final Culture Medium with a 1-mL Rainin pipette followed by a glass Pasteur pipette (resuspension volume varied by age and size of cortices). Final Culture Medium (made fresh on day of culture) was 2 mL 100× Na-Pyruvate (Invitrogen 11360–070), 2 mL 200 nM L-glutamine (Gibco A2916801), and 4 mL 50× B-27 without Vitamin A (Gibco 12587010) per 200 mL DMEM (Invitrogen 11960–051) filtered through a 0.22-μm cellulose acetate membrane (BD Biosciences 302995). After filtration, 100 μL 100× N2 (Invitrogen catalog no. 17502–048), 100 μL 100× *N*-acetyl-cysteine (Sigma catalog no. A-9165), and 20 μL 10 μg/mL basic fibroblast growth factor (Invitrogen catalog no. 13256–029) were added per 20 mL of medium. The cell suspensions sat at room temperature (20 °C) for 15 min to allow any cell clumps to settle to the bottom of the conical tube. Then, between 1 and 3 μL of cell suspension from the top of the tube was added to each well of the poly-L-lysine–coated Terasaki plates (Fisher catalog no. 07–000-401) to get a very low density. The Terasaki plates were pretreated with 1 mg/mL poly-L-lysine for 30 min, rinsed with water, and stored with 4 mL Base Culture Media at 4 °C until use. In the case of the NSC cultures, cells were plated at 50,000 cells per coverslip and cultured for 24 h before fixation. The plates were placed in a humidifying chamber and into a 37 °C incubator with 5% CO_2 for 20 h to allow one round of cell division. Afterward, the cells were fixed with 4% PFA for 2 min followed by 5 min for cold methanol (100% methanol at −20 °C) in −20 °C freezer. Immunostaining was followed as described below except that the plate was kept in a humidified chamber to prevent evaporation, and volumes of washes and antibodies were adjusted. Images were acquired using a Zeiss AxioZoom Observer.Z1 with a 40× air objective.

Antibodies and Immunofluorescence Staining. Following fixation, cortical slabs or dissociated NSCs cultured on coverslips (Fisher Brand Microscope Coverglass 18Cir-1D catalog no. 12–545-84) were incubated for 1 h at room

temperature (20 °C) in blocking buffer (0.1% Triton-X, 2 to 5% Normal Goat Serum in PBS) and then overnight at 4 °C or for 3 h at room temperature (20 °C) in the appropriate primary antibody solution (antibody diluted in blocking solution). After primary incubation, coverslips were rinsed in PBS (three times every 10 min), or slabs were rinsed in PBS-triton once followed by two PBS rinses and then, incubated at room temperature (20 °C) with appropriate secondary antibody solution (1:200 dilution) for 30 min (dissociated NSCs) or 45 min (cortical slabs) in the dark. Following final washes in PBS, coverslips were mounted onto glass slides with flurogel (Electron Microscopy Sciences 17985–10), or slabs were coverslipped (22 × 22 #1 cover glass; Curtin Matheson Scientific Inc. catalog no. 089–409) with Fluoromount (Vectashield 4–1000). Antibodies used were chicken anti-Nestin (Aves Lab; NES), rabbit or mouse anti-Tubb3 (TUJ1; Abcam rabbit 52623 and Biolegend mouse 801201), mouse anti-Citron kinase (CITK; BD Biosciences 611376), rabbit anti-Aurora B (AurKB; Abcam ab2254), mouse anti-Cep55 (Santa Cruz sc-377018), and rabbit anti-Survivin (Cell Signaling Technology 2808). For F-actin visualization, we used Phalloidin (ThermoFisher A12380).

Statistical Analyses. Statistical analyses were performed with Excel (Microsoft) and GraphPad Prism. A statistician was consulted regarding the abscission duration analyses; *t* test was used to compare averages for normal data. ANOVA was used for multiple comparisons in Fig. 5*B*. Nonnormal data were compared using Kolmogorov–Smirnov and Mann–Whitney tests. Categorical data were compared using Fisher's and χ^2 tests. The statistical tests used and *P* values calculated in each graph are indicated in the corresponding figures. All error bars are SEM.

Data Availability. Data are available on request to N.D.D.

ACKNOWLEDGMENTS. This work was supported by NIH Grants R01 NS076640 and R21 NS106162 (both to N.D.D.), and the Robert R. Wagner Fellowship (to K.C.M.). We thank Jessica Neville Little, Xiaowei Lu, Bettina Winckler, Ann Sutherland, Sarah Siegrist, Jung-Bum Shin, Maria Lehtinen, Anthony Lamantia, and their laboratories for advice and discussion. We thank Michael Fleming for Fig. 1*E* images.

1. N. D. Dwyer *et al*., Neural stem cells to cerebral cortex: Emerging mechanisms regulating progenitor behavior and productivity. *J. Neurosci.* **36**, 11394–11401 (2016).
2. S. Bizzotto, F. Francis, Morphological and functional aspects of progenitors perturbed in cortical malformations. *Front. Cell. Neurosci.* **9**, 30 (2015).
3. D. Jayaraman, B.-I. Bae, C. A. Walsh, The genetics of primary microcephaly. *Annu. Rev. Genomics Hum. Genet.* **19**, 177–200 (2018).
4. S. C. Noctor, V. Martínez-Cerdeño, A. R. Kriegstein, Distinct behaviors of neural stem and progenitor cells underlie cortical neurogenesis. *J. Comp. Neurol.* **508**, 28–44 (2008).
5. M. P. Postiglione *et al*., Mouse inscuteable induces apical-basal spindle orientation to facilitate intermediate progenitor generation in the developing neocortex. *Neuron* **72**, 269–284 (2011).
6. B. E. LaMonica, J. H. Lui, D. V. Hansen, A. R. Kriegstein, Mitotic spindle orientation predicts outer radial glial cell generation in human neocortex. *Nat. Commun.* **4**, 1665 (2013).
7. J. Yingling *et al*., Neuroepithelial stem cell proliferation requires LIS1 for precise spindle orientation and symmetric division. *Cell* **132**, 474–486 (2008).
8. Y. Feng, C. A. Walsh, Mitotic spindle regulation by Nde1 controls cerebral cortical size. *Neuron* **44**, 279–293 (2004).
9. R. A. Green, E. Paluch, K. Oegema, Cytokinesis in animal cells. *Annu. Rev. Cell Dev. Biol.* **28**, 29–58 (2012).
10. B. Mierzwa, D. W. Gerlich, Cytokinetic abscission: Molecular mechanisms and temporal control. *Dev. Cell* **31**, 525–538 (2014).
11. A. R. Skop, H. Liu, J. Yates, 3rd, B. J. Meyer, R. Heald, Dissection of the mammalian midbody proteome reveals conserved cytokinesis mechanisms. *Science* **305**, 61–66 (2004).
12. C. K. Hu, M. Coughlin, T. J. Mitchison, Midbody assembly and its regulation during cytokinesis. *Mol. Biol. Cell* **23**, 1024–1034 (2012).
13. C. Addi *et al*., The Flemmingsome reveals an ESCRT-to-membrane coupling required for completion of cytokinesis. bioRxiv:10.1101/2020.01.15.907857 (15 January 2020).
14. J. W. Connell, C. Lindon, J. P. Luzio, E. Reid, Spastin couples microtubule severing to membrane traffic in completion of cytokinesis and secretion. *Traffic* **10**, 42–56 (2009).
15. J. Guizetti *et al*., Cortical constriction during abscission involves helices of ESCRT-III-dependent filaments. *Science* **331**, 1616–1620 (2011).
16. E. F. Crowell, A. L. Gaffuri, B. Gayraud-Morel, S. Tajbakhsh, A. Echard, Engulfment of the midbody remnant after cytokinesis in mammalian cells. *J. Cell Sci.* **127**, 3840–3851 (2014).
17. E. Peterman *et al*., The post-abscission midbody is an intracellular signaling organelle that regulates cell proliferation. *Nat. Commun.* **10**, 3181 (2019).
18. M. Bernabé-Rubio *et al*., Novel role for the midbody in primary ciliogenesis by polarized epithelial cells. *J. Cell Biol.* **214**, 259–273 (2016).
19. L. K. Dionne, X. J. Wang, R. Prekeris, Midbody: From cellular junk to regulator of cell polarity and cell fate. *Curr. Opin. Cell Biol.* **35**, 51–58 (2015).
20. A. W. Ettinger *et al*., Proliferating versus differentiating stem and cancer cells exhibit distinct midbody-release behaviour. *Nat. Commun.* **2**, 503 (2011).
21. G. Pollarolo, J. G. Schulz, S. Munck, C. G. Dotti, Cytokinesis remnants define first neuronal asymmetry in vivo. *Nat. Neurosci.* **14**, 1525–1533 (2011).
22. V. Salzmann *et al*., Centrosome-dependent asymmetric inheritance of the midbody ring in Drosophila germline stem cell division. *Mol. Biol. Cell* **25**, 267–275 (2014).
23. D. Singh, C. Pohl, A function for the midbody remnant in embryonic patterning. *Commun. Integr. Biol.* **7**, e28533 (2014).
24. K. F. Lenhart, S. DiNardo, Somatic cell encystment promotes abscission in germline stem cells following a regulated block in cytokinesis. *Dev. Cell* **34**, 192–205 (2015).
25. T. C. Kuo *et al*., Midbody accumulation through evasion of autophagy contributes to cellular reprogramming and tumorigenicity. *Nat. Cell Biol.* **13**, 1214–1223 (2011).
26. A. Chaigne *et al*., Abscission couples cell division to embryonic stem cell fate. bioRxiv: 10.1101/798165 (8 October 2019).
27. K. M. Janisch *et al*., The vertebrate-specific Kinesin-6, Kif20b, is required for normal cytokinesis of polarized cortical stem cells and cerebral cortex size. *Development* **140**, 4672–4682 (2013).
28. J. N. Little, N. D. Dwyer, p53 deletion rescues lethal microcephaly in a mouse model with neural stem cell abscission defects. *Hum. Mol. Genet.* **28**, 434–447 (2019).
29. N. D. Dwyer *et al*., A forward genetic screen with a thalamocortical axon reporter mouse yields novel neurodevelopment mutants and a distinct emx2 mutant phenotype. *Neural Dev.* **6**, 3 (2011).
30. K. M. Janisch, K. C. McNeely, J. M. Dardick, S. H. Lim, N. D. Dwyer, Kinesin-6 KIF20B is required for efficient cytokinetic furrowing and timely abscission in human cells. *Mol. Biol. Cell* **29**, 166–179 (2018).
31. A. Abaza *et al*., M phase phosphoprotein 1 is a human plus-end-directed kinesin-related protein required for cytokinesis. *J. Biol. Chem.* **278**, 27844–27852 (2003).
32. O. Gershony, T. Pe'er, M. Noach-Hirsh, N. Elia, A. Tzur, Cytokinetic abscission is an acute G1 event. *Cell Cycle* **13**, 3436–3441 (2014).
33. N. Elia, R. Sougrat, T. A. Spurlin, J. H. Hurley, J. Lippincott-Schwartz, Dynamics of endosomal sorting complex required for transport (ESCRT) machinery during cytokinesis and its role in abscission. *Proc. Natl. Acad. Sci. U.S.A.* **108**, 4846–4851 (2011).
34. E. Daniel *et al*., Coordination of septate junctions assembly and completion of cytokinesis in proliferative epithelial tissues. *Curr. Biol.* **28**, 1380–1391.e4 (2018).
35. V. Dubreuil, A. M. Marzesco, D. Corbeil, W. B. Huttner, M. Wilsch-Bräuninger, Midbody and primary cilium of neural progenitors release extracellular membrane particles enriched in the stem cell marker prominin-1. *J. Cell Biol.* **176**, 483–495 (2007).
36. P. Luján *et al*., PRL-3 disrupts epithelial architecture by altering the post-mitotic midbody position. *J. Cell Sci.* **129**, 4130–4142 (2016).
37. X. Qian, S. K. Goderie, Q. Shen, J. H. Stern, S. Temple, Intrinsic programs of patterned cell lineages in isolated vertebrate CNS ventricular zone cells. *Development* **125**, 3143–3152 (1998).
38. M. L. Bondeson *et al*., A nonsense mutation in CEP55 defines a new locus for a Meckel-like syndrome, an autosomal recessive lethal fetal ciliopathy. *Clin. Genet.* **92**, 510–516 (2017).
39. F. Di Cunto *et al*., Defective neurogenesis in citron kinase knockout mice by altered cytokinesis and massive apoptosis. *Neuron* **28**, 115–127 (2000).
40. P. Frosk *et al*.; FORGE Canada Consortium; Canadian Rare Diseases: Models & Mechanisms Network, A truncating mutation in CEP55 is the likely cause of MARCH, a novel syndrome affecting neuronal mitosis. *J. Med. Genet.* **54**, 490–501 (2017).
41. H. Li *et al*., Biallelic mutations in citron kinase link mitotic cytokinesis to human primary microcephaly. *Am. J. Hum. Genet.* **99**, 501–510 (2016).
42. A. Moawia *et al*., Mutations of KIF14 cause primary microcephaly by impairing cytokinesis. *Ann. Neurol.* **82**, 562–577 (2017).
43. K. C. McNeely *et al*., Mutation of Kinesin-6 Kif20b causes defects in cortical neuron polarization and morphogenesis. *Neural Dev.* **12**, 5 (2017).
44. J. Lafaurie-Janvore *et al*., ESCRT-III assembly and cytokinetic abscission are induced by tension release in the intercellular bridge. *Science* **339**, 1625–1629 (2013).
45. V. Nähse, L. Christ, H. Stenmark, C. Campsteijn, The abscission checkpoint: Making it to the final cut. *Trends Cell Biol.* **27**, 1–11 (2017).
46. E. Petsalaki, G. Zachos, Building bridges between chromosomes: Novel insights into the abscission checkpoint. *Cell. Mol. Life Sci.* **76**, 4291–4307 (2019).
47. S. Y. S. Fung, M. Kitagawa, P. J. Liao, J. Wong, S. H. Lee, Opposing activities of Aurora B kinase and B56-PP2A phosphatase on MKlp2 determine abscission timing. *Curr. Biol.* **27**, 78–86 (2017).
48. A. Gromley *et al*., A novel human protein of the maternal centriole is required for the final stages of cytokinesis and entry into S phase. *J. Cell Biol.* **161**, 535–545 (2003).
49. J. G. Carlton, A. Caballe, M. Agromayor, M. Kloc, J. Martin-Serrano, ESCRT-III governs the Aurora B-mediated abscission checkpoint through CHMP4C. *Science* **336**, 220–225 (2012).
50. Y. Chai *et al*., Apoptotic regulators promote cytokinetic midbody degradation in C. elegans. *J. Cell Biol.* **199**, 1047–1055 (2012).
51. M. D. Muzumdar, B. Tasic, K. Miyamichi, L. Li, L. Luo, A global double-fluorescent Cre reporter mouse. *Genesis* **45**, 593–605 (2007).
52. S. Hayashi, P. Lewis, L. Pevny, A. P. McMahon, Efficient gene modulation in mouse epiblast using a Sox2Cre transgenic mouse strain. *Mech. Dev.* **119**, S97–S101 (2002).
53. P. Steigemann *et al*., Aurora B-mediated abscission checkpoint protects against tetraploidization. *Cell* **136**, 473–484 (2009).
54. K. M. Janisch, N. D. Dwyer, Imaging and quantitative analysis of cytokinesis in developing brains of Kinesin-6 mutant mice. *Methods Cell Biol.* **131**, 233–252 (2016).
55. K. F. Chau *et al*., Progressive differentiation and instructive capacities of amniotic fluid and cerebrospinal fluid proteomes following neural tube closure. *Dev. Cell* **35**, 789–802 (2015).
56. C. J. Bott *et al*., Nestin in immature embryonic neurons affects axon growth cone morphology and Semaphorin3a sensitivity. *Mol. Biol. Cell* **30**, 1214–1229 (2019).